International Journal of Impact Engineering 80 (2015) 36–44

Contents lists available at ScienceDirect

International Journal of Impact Engineering

journal homepage: www.elsevier.com/locate/ijimpeng

Prediction of the perforation of targets impacted by deformable projectiles

J. Baroth*, Y. Malecot, Z. Boukria, M. Briffaut, L. Daudeville

Université Joseph Fourier, Grenoble I, Grenoble INP, CNRS, 3SR Lab, BP53, 38051 Grenoble Cedex 9, France

ARTICLE INFO

Article history:
Received 9 October 2014
Accepted 12 January 2015
Available online 28 January 2015

Keywords:
Hard and soft impacts
Pendulum test
Reinforced concrete target
Perforation limit
Crushing force
Perforation

ABSTRACT

This paper proposes a simple formulation for the impact analysis of a deformable projectile on reinforced concrete targets. This approach assumes the presence of soft strikers and rigid targets. Based on an energy balance, it aims to predict a perforation limit for different targets under soft impacts. The procedure employed is validated by means of tests performed on a rigid target (pendulum test) and reinforced concrete slabs. The article discusses various estimations of the crushing force of projectiles, as derived from experimental results and numerical approaches. The efficiency of simplified approaches is highlighted from an engineering point of view. The limit between soft and hard impacts is also analyzed according to a recent criterion. Moreover, the paper proposes validating the approach using experimental tests with both perforating and non-perforating impact tests on nine slabs.

1. Introduction

The study of the mechanical response to loads generated by impacts is key to the analysis of structural vulnerability. Depending on the striker's strength, the phenomenon involved and therefore the target response may differ. Most of the existing empirical formulae used to predict perforation are proposed for the case of hard impacts on either reinforced concrete (RC) barriers [1,2] or metal targets, e.g. Ref. [3]. Few approaches are available to assess the possible perforation of a barrier subjected to a soft impact. In the case of an aircraft impact, Riera [4] considered the projectile as a two-body system: a crushed pipe with no velocity in contact with the structure, and a tube. The resulting contact force however still needs to be applied to a numerical model of the barrier in order to predict the perforation. CEB and Baroth et al. [5,6] proposed analytical formulae of ballistic velocities in the case of a soft missile impact on reinforced concrete targets. Baroth et al. [6] based their study on a collection of experimental data, as presented in Ref. [7]. Their findings highlight that the application ranges of most perforation formulae [1] must be considered with caution since such ranges often depend on the compressive strength of concrete after 28 days (f_{c28}), whereas various experimental results [8–10] demonstrate that concrete under high confinement becomes insensitive to f_{c28}.

The present work develops a simple analytical formulation of perforation models in the case of soft impacts. This formulation, based on an energy balance, yields a model aimed at predicting a perforation limit for different targets under soft impacts. This paper also discusses various estimations of the crushing force of projectiles, through reliance on experimental results and different numerical approaches. The limit between soft and hard impacts is also analyzed using the criterion developed by Koechlin [11].

Section 2 recalls and develops the formulation proposed in Ref. [6] and moreover specifies the crushing force calculations. This set of formulation and calculations are then applied to the experimental results of a pendulum test (Section 3). From the initial formulation, simple formulae are also deduced in order to predict the ballistic velocity limit and perforation limit in the case of a soft impact on reinforced concrete targets (Section 4). Lastly, Section 5 proposes a validation of the approach through an experimental campaign on both perforating and non-perforating impact tests [7].

2. Prediction of perforation in the case of soft impact

The first subsection (2.1) recalls and develops the premise proposed in Ref. [6]. It is complemented by potential calculations of the crushing force generated by the deformable projectile (subsection 2).

* Corresponding author. Fax: +33 476 827043.
E-mail address: jbaroth@ujf-grenoble.fr (J. Baroth).

http://dx.doi.org/10.1016/j.ijimpeng.2015.01.002
0734-743X/

2.1. The energy balance of a soft impact process

Let's consider a target of mass, M_T, under the impact of a projectile of mass M_P, total length L and diameter d. The projectile is assumed to be rigid over a length L_H. Let's begin by decomposing the impact process into three stages (see Fig. 1), with a distinction made between soft and hard impacts [12].

2.1.1. Stages of the impact process

During Stage 0, i.e. before the impact has occurred, the initial projectile velocity and kinetic energy are respectively denoted V_0 and E_{P0}.

Stage 1 corresponds to the soft part of the impact (crushed length $u < L-L_H$). The energy dissipated during the crushing phase, which lasts Δt, is defined as the mechanical work W_P done by the time-dependent crushing force $F_p(t)$ through the crushed length u_P of the projectile. The motion of the impacted target is characterized by: displacement u_T, velocity $\dot{u}_T$, acceleration $\ddot{u}_T$, and mechanical work W_T. At the end of Stage 1, i.e. after the crushing, the velocity and kinetic energy of the projectile are respectively denoted V_1 ($<V_0$) and E_{P1}. In Stage 2, the impact becomes hard (if the velocity is high enough). During perforation, the failure energy of the target E_F is dissipated. The projectile velocity and kinetic energy are now respectively denoted V_2 and E_{P2}. The velocity of the target V_T reaches its maximum value.

2.1.2. Energy balance during the perforation process

During Stage 1, the initial kinetic energy E_{P0} of the projectile is reduced to the kinetic energy E_{P1} after crushing of the deformable part of the projectile. The energy balance during the crushing process can be summarized by noting:

$$E_{P0} - E_{P1} = W_P + W_T \tag{2.1}$$

where E_{P0} and E_{P1} depend on the initial velocity V_0 and velocity V_1, in assuming the weight loss is insignificant during crushing, thus neglecting damage in the target throughout the phase:

$$E_{pi} = M_p V_i^2 \big/ 2, \quad i = 1, 2\ldots \tag{2.2}$$

The energy dissipated during the crushing phase, which lasts Δt, is defined by the mechanical work W_P done by the time-dependent crushing force $F_p(t)$ through the crushed length u of the projectile. Considering that the projectile can be modeled as a one-dimensional nonlinear spring, this mechanical work is written as:

$$W_P = \int_0^{\Delta t} F_p(t)\dot{u}_P(t)dt \tag{2.3}$$

where $\dot{u}_P(t)$ is the velocity of the projectile.

The mechanical work W_T relative to the motion of the target, whose mass is assumed constant, is expressed as follows:

$$W_T = M_T \int_0^{\Delta t} \ddot{u}_T(t)\dot{u}_T(t)dt \tag{2.4}$$

where $\ddot{u}_T(t)$ is the acceleration and $\dot{u}_T(t)$ the velocity of the impacted target.

At Stage 2, the initial kinetic energy E_{P1} of the projectile is reduced to the kinetic energy E_{P2} after perforation of the target by the crushed projectile:

$$E_{P0} - E_{P2} = W_P + W_T + E_F \tag{2.5}$$

E_F is the failure energy of the target, i.e. the energy dissipated during the perforation process. In the case of impact on a metal target, E_F can be found, for instance, in Ref. [3]. In the case of impact on a concrete target, E_F can be defined, according to the energy balance, such that

$$E_F = \frac{M_P\left(V_0^2 - V_2^2\right)}{2} - W_P - W_T - E_T \tag{2.6}$$

One difficulty encountered when using this approach is to estimate both the crushing force F_P of the projectile and the work W_P of this force over the crushed length. The following section will develop this point further. Afterwards, a pendulum test will be studied, with emphasis on estimating the crushing work of the projectile W_P and the crushing forceF_P.

2.2. Crushing force for a deformable projectile

The well-known Riera Model may be used to estimate the force $F_P(t)$ [4], bearing in mind that this model is not explicit, nor does it take into account the strain velocity effect and cylindrical projectile

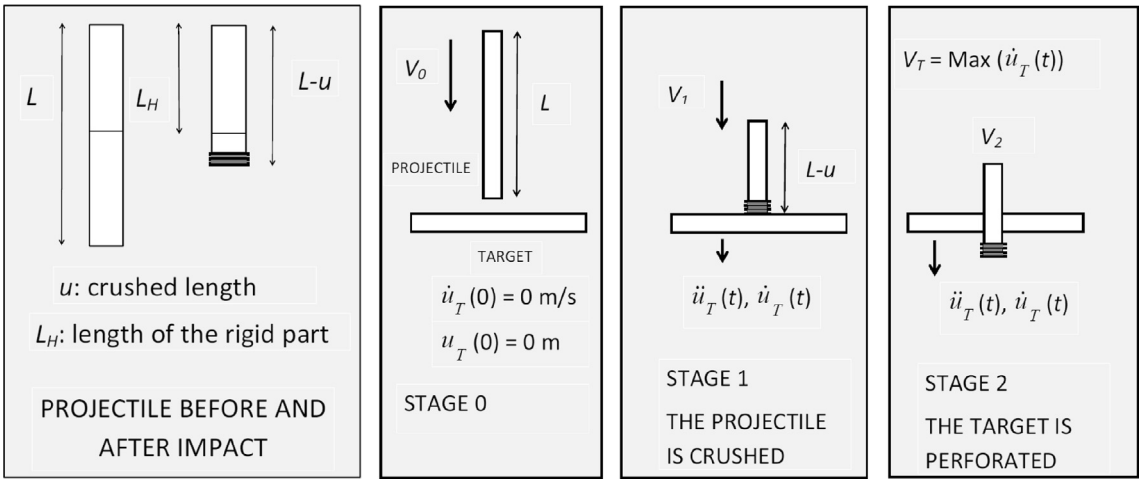

Fig. 1. Stages of the impact of a deformable projectile on a rigid target.

buckling. The crushing force for hollow metal tubes is also estimated by the following formula, based on Rankine's Equation [13]:

$$F_p = 2\pi e_P \left(\frac{\sqrt{2(1-\nu^2)}}{e_P E} + \frac{2}{d f_y} \right)^{-1} \tag{2.7}$$

where E is the Young's modulus (Pa), υ the Poisson's ratio, d the projectile diameter (m), f_y the projectile limit strength (Pa) (which can be replaced by the dynamic limit strength f_{yd}), and e_p the projectile thickness (m).

Since this approach does not take buckling into account, the following discussion will consider failure by both plasticization and buckling. When the circumferential slenderness of the projectile is very high, the buckling of the cylindrical shell under an axial load must be investigated; this instability is well known [14,15]. The crushing strength F_p thus depends on the critical elastic buckling stress σ_{cr}, such that:

$$F_p = \chi \sigma_{cr} = \chi \frac{E e_P}{r_P \sqrt{3(1-\upsilon^2)}} \tag{2.8}$$

where E and υ are respectively the Young's modulus and Poisson's ratio, r_p the mean radius of the cylinder, χ the buckling reduction factor for elastic-plastic effects in a buckling strength assessment deduced from large experimental tests. The coefficient χ is intended to take into account shell imperfections. These imperfections can indeed lead to axisymmetric buckling with a succession of rings. The estimation of χ has been detailed in Ref. [15] for general purposes. In this work, let's define respectively:

$$\bar{\lambda}_0 = 0.2 \text{ and } \bar{\lambda}_P = \sqrt{\alpha / 0.4} \tag{2.9}$$

as the squash and plastic limit relative slenderness values, where α is the elastic imperfection reduction factor in bucking. Above the squash limit relative slenderness value $\bar{\lambda}_0$, resistance reductions (due to either instability or change in geometry) occur. Let's define the relative slenderness:

$$\bar{\lambda} = \sqrt{f_y / \sigma_{xRc}} \tag{2.10}$$

with σ_{xRc}, i.e. the critical meridian buckling stress. In the case of long cylinders, the reduction factor α and stress σ_{xRc} are respectively defined as follows:

$$\begin{aligned} \alpha &= \frac{0.62}{1 + 1.91 \left(\frac{\sqrt{r_P}}{Q\sqrt{e_P}} \right)^{1.44}}; \\ \sigma_{xRc} &= \left[1 + \frac{0.2}{C_{xb}} \left(1 - \frac{2Le_P}{r_P \sqrt{r_P e_P}} \right) \right] \frac{E e_P}{r_P \sqrt{3(1-\upsilon^2)}} \end{aligned} \tag{2.11}$$

where C_{xb} is a coefficient related to boundary conditions (between 1 and 6) and Q the value of fabrication quality (between 16 and 40 for normal and excellent qualities). If the relative slenderness $\bar{\lambda}$ lies between $\bar{\lambda}_0$ and $\bar{\lambda}_P$, then the coefficient χ (see (2.8)) is written as:

$$\chi = 1 - \beta \frac{\bar{\lambda} - \bar{\lambda}_0}{\bar{\lambda}_P - \bar{\lambda}} \tag{2.12}$$

where β is the plastic range factor in buckling interaction, equal to 0.6 in this work [15] (Table 1).

3. Ballistic pendulum test

3.1. Experimental set-up

A steel cylindrical projectile with cross-sections of various thicknesses is launched onto a target using a 90-mm caliber gas gun (Fig. 2). The front part of the projectile is composed of a thin S235 steel tube (Table 2), which has a thickness of $e_{P1} = 1$ mm over the

Table 1
Main physical quantities, their units and the coefficients used.

Symbol	Parameter	Unit	Symbol	Parameter	Unit
M_p	Projectile mass	kg	χ	Buckling reduction factor of F_p	–
d	Projectile diameter	m	α	Meridian elastic imperfection ratio	–
L	Projectile length	m			
L_H	Length of the rigid projectile part		$\bar{\lambda}_0$	Squash limit relative slenderness	–
L_1	Length of 1-mm thick part of the projectile	m	$\bar{\lambda}_P$	Plastic limit relative slenderness	–
L_2	Length of 2-mm thick part of the projectile	m	$\bar{\lambda}$	Relative slenderness of the shell	–
u, u_1, u_2	Crushed lengths	m	σ_T	Compressive strength of the target	Pa
u^*	Characteristic crushed length	m	C_{xb}	Coefficient in the buckling assessment	–
F_P	Projectile crushing force	N	f_y	Yield strength	Pa
F_{P1}, F_{P2}	Projectile crushing forces (parts 1 and 2)	N	f_{yd}	Yield strength accounting for the strain velocity effect	Pa
A_P, A_{P1}, A_{P2}	Crushed projectile cross-sections (parts 1 and 2)	m^2	Q	Parameter for the effect of boundary conditions	–
e_{P1}, e_{P2}	Projectile thicknesses	m	E_T	Kinetic energy of the target	J
r_{P1}, r_{P2}	Projectile mean radius (parts 1 and 2)	m	f_u	Ultimate strength of the target material	Pa
V_0, V_0^*	Projectile velocity before impact, ballistic value	m/s	ε_u	Ultimate strain of the target material	–
V_1, V_1^*	Crushed projectile velocity at impact, ballistic value	m/s	E_F	Failure (perforation) energy of the target	J
V_2	Projectile velocity after impact	m/s	M_a	Reinforcement density	–
V_T	Final velocity of the target	m/s		RC target	
u_P,u_T	Displacements of the projectile and target	m	ω	Relative length of the shell	–
$\dot{u}_P$, $\dot{u}_T$	Velocities of the projectile and target	m/s	β	Plastic range factor in buckling interaction	–
$\ddot{u}_P$, $\ddot{u}_T$	Accelerations of the projectile and target	m/s^2	f_{c28}	Compressive strength of concrete (28 days, uniaxial)	Pa
ρ_p	Projectile mass density	kg/m^3	W_T	Mechanical work (target)	J
E_{pi}, $i=1,2,3$	Projectile kinetic energies relative to V_0, V_1, V_2	J	E_F	Failure energy (target)	J
W_P	Mechanical work (projectile)	J	M_T	Target mass	kg
υ	Poisson's ratio of steel	–	ρ_T	Target mass density	kg/m^3
E	Young's modulus of steel	Pa	e_T	Target thickness	m
σ_{cr}	Critical elastic buckling stress	Pa	e_T^*	Perforation limit	m
$\sigma_{x,Rc}$	Critical meridian buckling stress	Pa			

Fig. 2. Gas launcher, deformable projectile and ballistic pendulum device (just before impact) [7].

Table 2
Characteristics of all projectiles.

Symbol	Parameter	Value	Unit	Symbol	Parameter	Value	Unit
f_y	Yield strength	235	MPa	d	External diameter	80	mm
L	Length	500	mm	e_{P1}	Thickness (part 1)	1	mm
ρ_P	Mass density	7850	kg/m^3	e_{P2}	Thickness (part 2)	2	mm
υ	Poission's ratio	0.3	–	r_{P1}	Mean radius (part 1)	39.5	mm
E	Young's modulus	210	GPa	r_{P2}	Mean radius (part 2)	39	mm

first (L_1) front part and a thickness of e_{P2} = 2 mm over the remaining (L_2) part (Fig. 3). The third and rear part of the projectile is composed of a massive 35NCD16 steel cylinder incorporating an acceleration recording system designed to measure axial accelerations during the tests.

The ballistic pendulum test [7] consists of launching a deformable steel projectile (Tables 2 and 3) onto a massive rigid body (Table 3) hung to the ceiling with two 2-m long steel cables (Fig. 2). A non-deformable target, which is relatively heavy in comparison with the projectile mass, has been used to facilitate the crushing of the soft projectile on this rigid target. During the projectile crushing phase, the load is transferred to the rigid mass, which in turn is accelerated. LVDT and acceleration sensors have been positioned on the rear face of the steel block to measure displacement and velocity.

In this experiment, a projectile of length L has been launched with an initial striking velocity V_0. The projectile is a metal cylinder, whose thinner thickness is 1 mm over a 25-cm length and 2 mm over a 30-cm length. Fig. 3 shows the residual shape of the projectile at the end of the test. A series of regular plies are observed to have formed on the steel tube. The projectile residual lengths were also measured (Table 3).

Eq. (2.8) enables estimating the crushing strengths: F_{p1} over the 1-mm thick part of the projectile for lengthu_1; and F_{p2} over the 2-mm thick part of the projectile for length u_2 (Table 3). The mechanical work W_P done by the presumed constant crushing forces F_{p1} and F_{p2} can be approximated through the crushed lengths u_1 and u_2 of the projectile, in assuming that F_{p1} and F_{p2} remain constant.

$$W_P = F_{p1}u_1 + F_{p2}u_2 \tag{3.1}$$

3.2. Analytical estimation of the pendulum displacement

The energy balance (2.1) can be simplified by assuming a projectile velocity after crushing equal to the velocity of the target, as well as a zero failure energy E_F of the target. Energy balances need to be expressed. The first variation in kinetic energy (Eq. (2.2.)), $E_{P0}-E_{P1}$, is equal to the mechanical work W_P due to crushing of the projectile (Eq. (3.1.)). The next variation in kinetic energy $E_{P1}-E_{P2}$ is equal to the mechanical work W_T due to motion of the target (and the presumed embedded crushed projectile). The following energy balance can then be deduced:

$$\frac{1}{2}M_P V_0^2 - \frac{1}{2}(M_T+M_P)V_T^2 = F_{p1}u_1 + F_{p2}u_2 + u_T(M_T+M_P)\ddot{u}_T \tag{3.2}$$

Table 4 lists minimum and maximum values of the initial kinetic energy E_{P0} of the projectile and the kinetic energy E_T of the pendulum. The work resulting from the pendulum motion lasts 5 ± 0.3 ms, before the velocity $\dot{u}_T$ of the pendulum remains constant and equal to V_T.

Fig. 5 demonstrates that the evolution in motion is mainly linear. A mean acceleration $\ddot{u}_T$ of 640 m/s^2 is therefore deduced.

The calculated lower and upper bounds of u_T, in taking experimental uncertainties and buckling into account, are found to lie between 4.5 and 9 cm (Table 4), whereas the measured distance u_T is greater than 5 cm (due to a lack of precision in the displacement sensor). The experimental measurement, slightly over 5 cm, is included within this interval. Crushing strengths F_{p1} and F_{p2} are respectively estimated using Bignon & Riera [13] and EC3 approaches (Table 5).

In accounting for estimation accuracy (Table 4), Eurocode 3 [15] provides a relevant pendulum test forecast, although Bignon & Riera [13] propose a slightly underestimated displacement. The method that takes buckling into account thus seems to be more accurate than Bignon's formula (Eq. (2.7)). From Table 4,

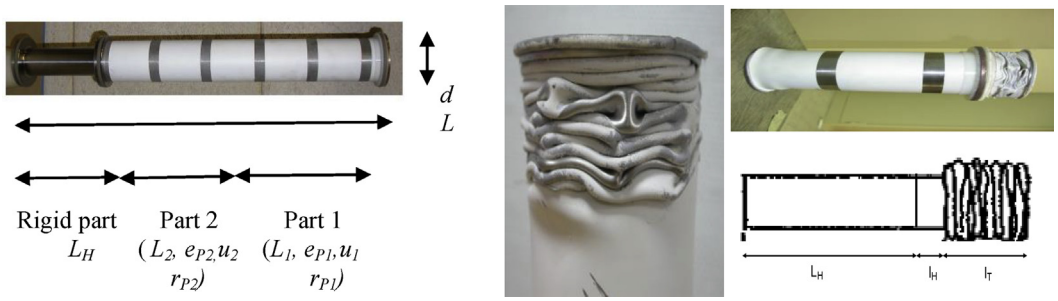

Fig. 3. Projectile dimensions and post-test deformation [7].

Table 3
Ballistic test: Specific characteristics of both the projectile and target, and test results.

Symbol	Parameter	Value	Unit	Symbol	Parameter	Value	Unit
M_P	Projectile mass	5.027	kg	M_T	Target mass	153	kg
V_0	Velocity before impact	89.2+/1	m/s				
F_{p1}	Crushing strength (part 1)	47.5	kN	u_1	Crushed length	21 ± 0.5	cm
F_{p2}	Crushing strength (part 2)	99.6	kN	u_2	Crushed length	3 ± 0.5	cm

Table 4
Estimation of the impact characteristics and pendulum displacement (min and max values and variations around mean values).

Symbol	Parameter	Unit	Min	Max	Variation (%)
M_T	Pendulum mass	kg	152.5	153.5	±0.3%
V_0	Initial projectile velocity	m/s	88.2	90.2	±1.1%
C_{xb}	Boundary conditions parameter	–	1	6	±71%
Q	Fabrication quality parameter	–	16	40	±43%
E_{P0}	Initial projectile kinetic energy	J	19,554	20,451	±2.2%
W_P	Mechanical work (Eq. (3.1))	J	11,992	13,938	±7.5%
E_T	(Pendulum + projectile) kinetic energy	J	782	837	±3.4%
$\ddot{u}_T$	(Pendulum + projectile) acceleration	m/s^2	590	690	±7.8%
V_T	Final (pendulum + projectile) velocity	m/s	3.15	3.25	±1.6%
u_T	(Pendulum + projectile) displacement	cm	4.3	8.7	±34%

parameters for the effect of projectile fabrication quality and boundary conditions are particularly scattered. To ensure method robustness, the influence of these parameters is evaluated using EC3. Table 6 indicates that this influence appears to be quite insignificant.

3.3. Numerical application

A simulation of the ballistic pendulum test was conducted using the Abaqus/Explicit finite element code (version 6.10) in order to compare numerical and experimental results, as well as validate the crushing force approximation. The projectile is discretized by 4-node shell elements with reduced integration, the steel block by 3D volume elements with reduced integration, and the cables by bar elements. The behavior of the material along the front part of the projectile (S235) has been modeled by the Johnson-Cook Law [16] in taking strain velocity effects into account:

$$\sigma = \left[A + B\left(\bar{\varepsilon}_{pl}\right)^n\right]\left[1 + C\,Ln\left(\frac{\dot{\bar{\varepsilon}}_{pl}}{\dot{\varepsilon}_0}\right)\right] \tag{3.3}$$

with: $A = 480$ MPa, $B = 300$ MPa, $C = 0.12$, $n = 0.36$.

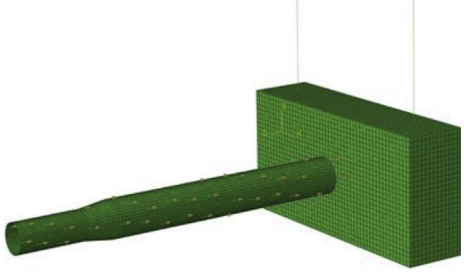

Fig. 4. Ballistic pendulum test simulation.

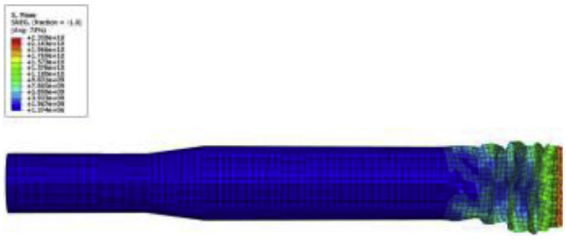

Fig. 5. Projectile after impact.

The massive rear part of the projectile and steel block is assumed to be perfectly elastic; the guide ring has been modeled by aluminum with a thickness adapted to match the actual mass (Fig. 4). The weight of each component is verified (to match experimental results), and the projectile velocity is initialized to $V_0 = 89.2$ m/s.

Like in the test, a series of plies forms on the steel tube during the projectile crushing process (Fig. 5) over the thinner part of the projectile (1-mm thick). Only 6 plies are formed instead of the 13 observed experimentally. Fig. 6 shows a comparison of changes in the projectile velocity obtained both experimentally (by integrating the acceleration signal) and numerically (from average velocity at the nodes located on the rear part of the projectile).

Fig. 6 displays a comparison of the change in target velocity between experimental findings (by deriving the displacement signal) and numerical results (from the kinetic energy of the steel block). Fig. 7 shows the evolution in mechanical work done by crushing forces F_{p1} and F_{p2} vs. the crushed length u of the projectile. After about 5 ms, the crushing phase is complete and the crushed length equals about 31 cm; the work can be deduced from Eq. (2.3). Both the measured and numerical works are close. Their evolution is rather linear, until a decrease explained by the end of pendulum motion. Riera and Bignon [13] and Eurocode approaches are also shown. Although Riera overestimates the final work, analytical and explicit approaches, such as Bignon and Eurocode, are closer to the final measured work. A simplified approach therefore seems reasonable from an engineering point of view.

4. Prediction of perforation in the case of a soft impact on reinforced concrete barriers

In this section, the motion of the target is assumed to be insignificant (i.e. $V_T = 0$). The energy balance (1) can then be simplified.

$$E_{P0} = W_P + E_F + E_{P2} \tag{4.1}$$

Let's write once again this energy balance using Eq. (2.2).

Table 5
Estimation of pendulum displacement (average values, cm) for two estimations of crushing strength.

Approach	F_{p1} (kN)	F_{p2} (kN)	Estimation	Experiment
EC3	47.5	99.6	6.5 ± 2 cm	>5 cm
Bignon & Riera	53	112	4.8 ± 2 cm	

Table 6
Estimation of mean pendulum displacement for various parameters for the effect of fabrication quality (Q) and boundary conditions (C_{xb}).

	Fabrication quality		Boundary conditions	
	Min ($Q = 16$)	Max ($Q = 40$)	Min ($C_{xb} = 1$)	Max ($C_{xb} = 6$)
Average parameters	$C_{xb} = 3$		$Q = 25$	
Average pendulum displacement	6.4 ± 2 cm	6.5 ± 2 cm	6.3 ± 2 cm	6.5 ± 2 cm

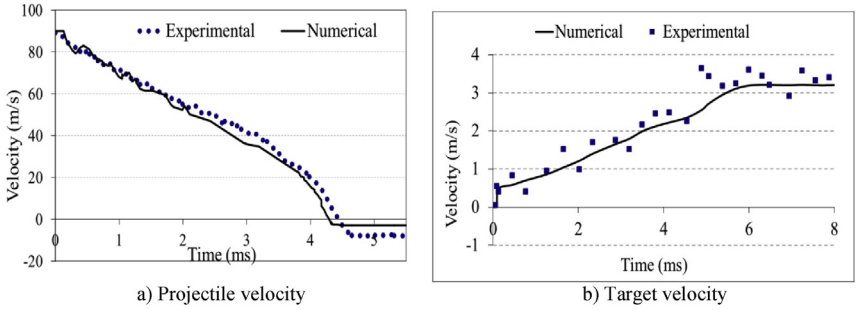

a) Projectile velocity b) Target velocity

Fig. 6. Comparison of numerical vs. experimental velocities.

$$M_p V_0^2/2 = W_p + E_F + M_p V_2^2/2 \tag{4.2}$$

From this energy balance, simple formulae are deduced to predict the ballistic limit (subsection 1), the characteristic crushed length of the projectile (subsection 2), and the perforation limit of reinforced concrete barriers (subsection 3).

4.1. Ballistic limit prediction in the case of a soft impact on RC targets

In the case of a soft impact on a concrete target, a limit case can be defined for which the target is perforated with no residual velocity for the projectile ($V_2 = E_{P2} = 0$). In such a case, the initial velocity V_0 is equal to the ballistic limit V_0^* of the target for the given projectile. Let's assume that the failure (perforation) energy E_F of the target equals the residual kinetic energy once the projectile has been crushed. Eq. (4.2) then becomes:

$$Mp\left(V_0^*\right)^2/2 = W_p + M_p\left(V_1^*\right)^2/2 \tag{4.3}$$

where V_1^* is the ballistic limit of the crushed projectile. According to the definition of Stage 2 of the perforation process (Fig. 1), a sudden perforation occurs and a hard impact can be considered. For such impacts, the ballistic limits have been widely published [1].

A general, but simple, expression of the ballistic limit V_0^* can then be deduced from Eq. (4.3):

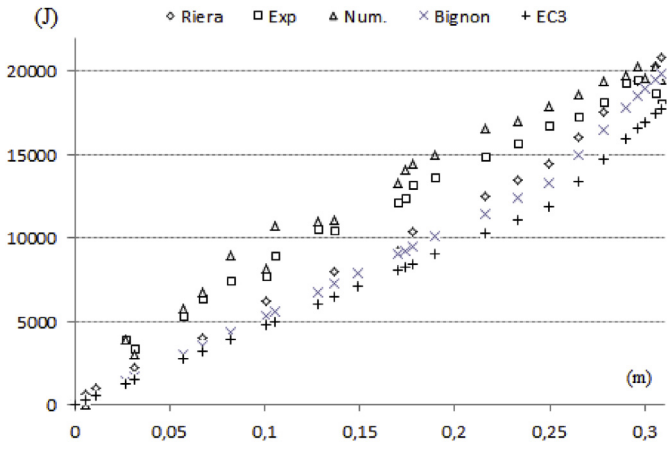

Fig. 7. Mechanical work W_P done by crushing forces vs. crushed length, using Bignon and Eurocode formulae, plus the Riera method; comparison with experimental and numerical results.

$$V_0^* = \sqrt{\left(V_1^*\right)^2 + \frac{2W_p}{M_P}} \tag{4.4}$$

The well-known Riera model [4] or more simplified approaches [13,15] can be applied at this point to estimate the force $F_p(t)$ [4] and energy W_p using Eq. (2.3) or Eq. (3.1).

Baroth et al. [6] proposed a ballistic limit close to that in Eq. (4.4) for the purpose of evaluating the ballistic velocity of a deformable cylindrical projectile, in assuming that work W_p can be written: $W_p = F_p u^*$, where u^* is the characteristic crushed length beyond which the impact becomes hard. This step is equivalent to averaging the crushing force exerted by the projectile on the target during the crash. The notion of averaging this force is also found in Refs. [5]; however, the characteristic crushed length of the projectile u^* still has to be estimated.

4.2. Estimation of a characteristic crushed length of the projectile u^*

To predict the occurrence of a hard impact (Stage 1, Fig. 1), a condition between hard and soft impacts has been proposed and illustrated on aircraft crashes by Koechlin [11]. Given V_1^* as the ballistic limit of the target for the crushed projectile, this condition is expressed as:

$$\frac{\sigma_P}{\sigma_T} + \frac{\rho_P\left(V_1^*(u^*)\right)^2}{\sigma_T} = 1 \tag{4.5}$$

where σ_T is the compressive strength of the target (MPa), σ_p the compressive strength of the projectile (MPa), and ρ_p the mass density (kg/m^3). The strength σ_p can be written as: $\sigma_P = F_P/A_p$, where F_P and A_P are respectively the crushing force and cross-section of the crushed projectile.

Using this criterion along with Eqs. (4.4) and (4.5), the characteristic crushed length u^* is:

$$u^* = \mathrm{Max}\left(0, \frac{\mathrm{M_p}}{2\mathrm{F_p}}\left(\left(V_0^*\right)^2 - \frac{\sigma_T - F_p/A_p}{\rho_p}\right)\right) \tag{4.6}$$

If $u^* < u$, the dissipated energy during crushing is too high to allow perforation. Otherwise, if $u^* > u$, the dissipated energy during crushing is not high enough to stop the projectile.

4.3. Perforation limit of RC barriers

The perforation limit e_T^*, i.e. the minimum thickness of the target that allows resisting perforation, can also be deduced from Eq. (4.4), since the ballistic limit is typically correlated with the target thickness. For example, let's consider the well-known empirical

Table 7
Validity ranges for parameters used in Eq. (4.7) (min and max values).

Symbol	Parameter	Min	Max	Unit
d	Diameter	10	30	cm
f_{c28}	Uniaxial compressive strength of concrete after 28 days	30	45	MPa
M_a	Reinforcement density	150	250	kg/m^3
M_P	Projectile mass	30	300	kg
V_1	Projectile velocity - ballistic limit	20	250	m/s
e_T^*	Thickness of the target	10	60	cm
r_d	Reinforcement ratio	0.5	0.8	%
d/e_T^*	Projectile/target dimension ratio	0.5	1.5	–
$M_P/\rho_T(e_T^*)^2$	Projectile/target mass ratio	0.5	1.5	–

formula [17], which yields the ballistic limit in the case of hard impact from a cylindrical projectile of diameter d:

$$V_1^* = 1.3\rho_T^{1/6} f_{c28}^{0.5}\left(\frac{d(e_T^*)^2}{M_P}\right)^{2/3} \tag{4.7}$$

where all parameters are assumed to be valid (to within 10% accuracy) for the following range of variables (Table 7):

The perforation limit e_T^*, taking into account Eqs. (4.4) and (4.7), is deduced as follows.

$$e_T^* = 0.82\sqrt{\frac{M_T}{d}}\left(\frac{\left(V_0^*\right)^2 - \frac{2W_P}{M_T}}{\rho_T^{1/3} f_{c28}}\right)^{3/8} \quad \text{if} \tag{4.8}$$

$$E_{p0} = \frac{1}{2}M_P V_0^2 > W_p, \quad \text{but} \quad e_T^* \geq 0$$

The following section will present the experimental tests on soft impacts, whose results allow estimating the limit perforations of concrete targets.

5. Soft impact on a concrete slab

5.1. Experimental set-up

Nine cylindrical projectiles, whose common characteristics have already been presented (see Fig. 3), are launched on targets by a gas gun (Fig. 2). These targets are 2 m × 1.2 m rectangular reinforced concrete slabs with a thickness e_T of 7 or 6 cm and a mass density ρ_T. These slabs have been designed to simulate soft projectile impacts. The projectile velocity has in fact been changed in order to obtain various damage levels, ranging from slight bending to projectile perforation (Fig. 8).

Table 8
Data common to all nine reinforced concrete slabs [7].

Parameter	Value	Units	Parameter	Value	Units
ρ_T	2278	kg/m^3	r_d (e_T = 6 cm)	1	%
f_{c28}	28.6	MPa	r_d (e_T = 7 cm)	1.2	%

The target is tightly clamped by a metal support, assumed to be perfectly rigid. The nine tests were performed with different impact velocities, extending from 70 to 135 m/s (Table 9). Only the mass slightly changes from one projectile to another (Table 9). Test characteristics have been compiled in Tables 8 and 9. Most of the following data can be found in Refs. [6,7].

5.2. Comparison of perforation model forecasts with experimental results

Fig. 9 compares the slab thickness (70 or 60 mm) with the perforation limits estimated for each test. These limits have been estimated from Eq. (4.8), in considering three values of mechanical work W_P:

(i) W_P=0 corresponds to the case of a hard impact assumption (white dots);
(ii) W_P=L_1u_1 corresponds to the case of a soft impact assumption, for which only the thinnest part of the projectile is entirely crushed (diamonds);
(iii) W_P=$F_{p1}u_1$+$F_{p2}u_2$ corresponds to the case of a soft impact, for which the experimental crushed values (Table 6) of both deformable parts u_1 and u_2 of the projectile are used (Eq. (3.1)) (black dots).

Let's remark that the perforation forecast is satisfactory only if crushing has been taken into account (i.e. assumptions (ii) and (iii)). It should be specified that while a perforation has been accurately predicted in test 6, the experiment indicates that only concrete is crushed as the projectile is effectively stopped by the steel rods.

Fig. 10 presents the evolution in perforation limit e_T^* vs. crushed length u for various tests (1–9). This evolution has been deduced from Eq. (4.8), in which mechanical work can be expressed as:

$$W_P(u) = F_{p1}u_1 + F_{p2}u_2, \text{ with } u = u_1 \quad \text{if } u \in [0; 0.25\text{m}] \text{ and } u = 0.25 + u_2 \quad \text{if } u > 0.25\text{m}. \tag{5.1}$$

In the special case of Vulcain tests [7], two parts of the projectile can actually be potentially crushed, the first one over a 25-cm length (e_p = 1 mm) and the second over a 25-cm length (e_p = 2 mm).

Fig. 8. Reinforced concrete slabs both before and after impact [7].

Table 9
Specific data concerning each of the nine Vulcain tests [7].

Test	1	2	3	4	5	6	7	8	9
M_P (kg)	6.166	5.2073	5.0916	5.0728	5.0594	4.9853	5.0509	5.0653	5.0596
e_T (m)	0.07	0.07	0.07	0.06	0.07	0.07	0.07	0.07	0.07
V_0 (m/s)	135.5	107	92	89	73	93	80	70	68
u_1 (cm)	17	24	17	11.5	24	24.5	24	13	14
u_2 (cm)	0	5	0	0	0	0	0	5	5

Fig. 10 also shows the absence of perforation if the perforation limit exceeds slab thickness. If e_T^* decreases to this thickness, then a significant probability of perforation exists. An example of intersection between thickness and e_T^* for test 2 is also displayed: it provides the characteristic crushed length $u^* = u_1^* + u_2^* = 37$ cm (Fig. 10) for this test. The experimental value of $u_1+u_2 = 29$ cm (Table 6) is less than u^*, and indeed in test 2 the slab has been perforated. The energy dissipated during crushing is not sufficient to stop the projectile. As a contrast, the change in e_T^* for perforation test 7 has also been included, yielding the characteristic crushed length $u^* = u_1^* + u_2^* = 23$ cm (Fig. 10) for this same test. The experimental value of $u_1+u_2 = 24$ cm (Table 6) is greater than u^*, with the dissipated energy being too strong to enable perforation: the projectile is in fact stopped.

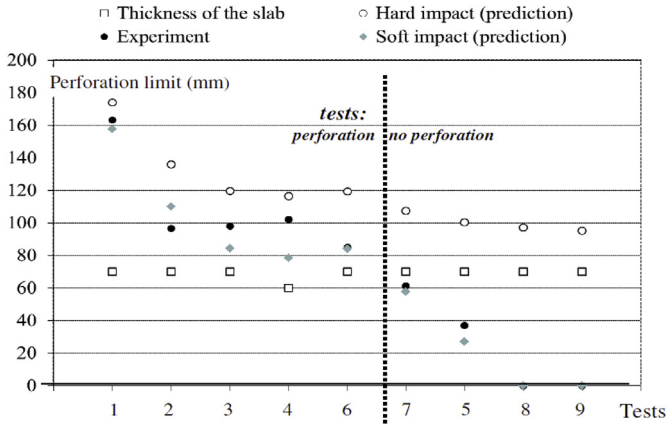

Fig. 9. Measured and estimated perforation capacities (soft impacts, mm).

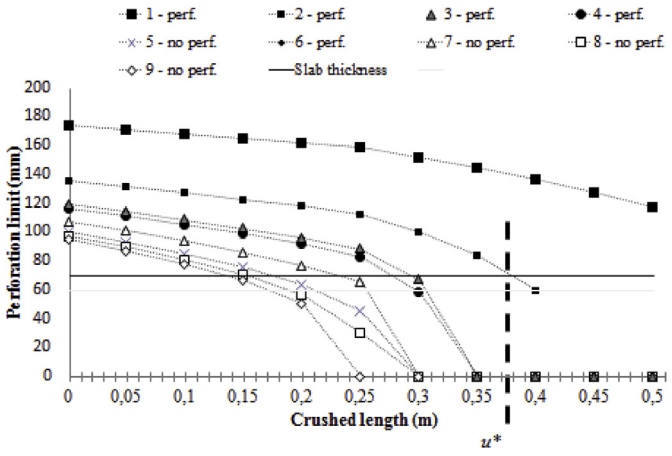

Fig. 10. Perforation limits for 9 Vulcain tests [6,7] according to different crushed lengths – Example of characteristic length u^* for perforation test 2 ($e_p = 70$ mm, $u^* = 37$ cm).

The characteristic crushed length u^* can be also estimated from Eq. (4.6) in the case of Vulcain tests [6,7]:

$$u^* = \mathrm{Max}\left(0;0{,}25 + \frac{M_p}{2F_{p_2}}\left(V_0^2 - \frac{F_{p1}}{2M_p} - \frac{\sigma_T - F_{p_1}/A_{p_1} - F_{p_2}/A_{p_2}}{\rho_p}\right)\right) \tag{5.2}$$

where M_P is the projectile mass, V_0 the initial velocity, and F_{p_1}, F_{p_2} the crushing forces of deformable projectile parts.

It can be a complicated process to estimate the compressive strength of the target σ_T since the impact generates confinement in concrete structures, thus making this strength apparently difficult to measure. Recent studies however on the same concrete used in these tests (R30A7) have allowed estimating the triaxial strength of a concrete specimen under high confinement [8,10,18]. Given that testing has been conducted about 1 month after slab construction, i.e. in the case of the saturated R30A7 specimen, the shear strength of concrete is limited to approx. 200 MPa, regardless of the level of confinement.

Table 10 presents the measured crushed lengths u (cm) (row 1) and characteristic crushed lengths u^* (cm) (rows 2–4) for 9 Vulcain tests [7], featuring different values of the compressive strength of concrete. This table shows that when using the normalized uniaxial compressive strength of concrete after 28 days, f_{c28}, as the characteristic compressive strength in the impact structure, σ_T is not satisfactory for accurately predicting the crushed length. In the event of an impact, a confinement pressure generated by inertia forces indeed increases the compressive strength of concrete. A higher value, found experimentally around 200 MPa, allows determining the correct order of magnitude. It can be verified that the characteristic values of u^* are then close to those listed in Fig. 10, which are also close to the experimental results.

6. Conclusion

This study has proposed a simple formulation for the impact analysis of a deformable projectile on reinforced concrete targets. The approach has been illustrated by recent experimental tests conducted on a steel pendulum and reinforced concrete slabs.

Based on the pendulum test, various estimations of the crushing force of projectiles have been proposed. For this case, simplified approaches [13,15] provide estimations on the order of experimental test findings and refined finite element simulations. From a simple energy balance perspective, it becomes possible to predict

Table 10
Measured crushed lengths u (cm) (row 1) and characteristic crushed lengths u^* (cm) (rows 2–4) for 9 Vulcain tests [7], with different values of the compressive strength of concrete.

σ_T/Tests	1	2	3	4	5	6	7	8	9
[Fig. 10]	>50	37	29	27	17	28	23	16	15
$f_{c28} \approx 29$ MPa	131	96	87	85	79	86	81	78	77
200 MPa	59	36	28	27	20	28	23	19	18
210 MPa	54	33	25	23	17	25	20	16	15

the perforation limits for various targets under soft impacts. Using a condition between hard and soft impacts [11], a characteristic crushed length has been defined. This theoretical value was then compared to a number of measured crushed lengths. Such a comparison yielded a value of the characteristic compressive strength in the concrete target of close to 200 MPa, which is the experimental strength measured on a concrete specimen under high triaxial loading [8–10]. The validation of this approach on a very large scale, such as the simulation of an aircraft crash on a nuclear containment structure [18], still needs to be completed.

In the future, this approach should be applied to other experimental tests (Meppen [19], Iris [20,21]). Steel structures should also be studied in using the perforation energy formulation given in Ref. [3].

Acknowledgments

The GIGA press has been installed in the 3SR Laboratory within the scope of a cooperative agreement with the CEA-Gramat facility. This research has been partially performed with the financial support of the French Ministry of Defense (DGA). Dr. Pontiroli (CEA-Gramat) is hereby acknowledged for managing the tests run on slabs. The contribution of the French Research Agency (ANR PGCU 2007) is also gratefully appreciated.

References

[1] Li QM, Reid SR, Wen HM, Telford AR. Local impact effects of hard missiles on concrete targets. Int J Impact Eng 2005;32(1–4):224–84.
[2] Buzaud E, Cazaubon C, Chauvel D. Assessment of empirical formulae for local response of concrete structures to hard projectile impact. In: Proc. CONSEC 07, Tours, France; 2007. p. 1365–72.
[3] Mebarki A, Nguyen QB, Mercier F, Ami Saada R, Meftah F, Reimeringer M. A probabilistic model for the vulnerability of metal plates under the impact of cylindrical projectiles. J Loss Prev Process Ind 2007;20(2):128–34.
[4] Riera JD. On the stress analysis of structures subjected to aircraft impact forces. Nucl Eng Des 1968;8(4):415–26.
[5] CEB. Concrete structures under impact and impulsive loading. Lausanne, Switzerland: Comité Euro-International du Béton, Bulletin d'Information; 1988. p. 87.
[6] Baroth J, Daudeville L, Malecot Y. About empirical models predicting the missile perforation of concrete barriers. Eur J Environ Civ Eng 2012;16(3):1074–89.
[7] Pontiroli C, Rouquand A, Baroth J, Daudeville L. Soft projectile impacts analysis on thin reinforced concrete slabs: tests, modelling and simulations. Eur J Environ Civ Eng 2012;16:1058–73.
[8] Gabet T, Malecot Y, Daudeville L. Triaxial behaviour of concrete under high stresses: influence of the loading path on compaction and limit states. Cem Concr Res 2008;38(3):403–12.
[9] Vu XH, Malecot Y, Daudeville L, Buzaud E. Effect of the water/cement ratio on concrete behaviour under extreme loading. Int J Numer Anal Methods Geomech 2009;33:1867–88.
[10] Poinard C, Malecot Y, Daudeville L. Damage of concrete in a very high stress state: experimental investigation. Mater Struct 2010;43:15–29.
[11] Koechlin P, Potapov P. Classification of soft and hard impacts – application to aircraft crash. Nucl Eng Des 2009;239:613–8.
[12] Eibl J. Soft and hard impact. Concrete for hazard protection. Edinburgh, UK: Concrete Society; 1987. p. 175–86.
[13] Bignon PG, Riera JD. Verification of methods of analysis for soft missile impact problems. Nucl Eng Des 1980;60(3):311–26.
[14] CECM. Recommendations of steel shells. Brussels: European Comittee for Standardization; 1988. p. 93. Publication CECM no. 56.
[15] EN 1993-1-1. (English): Eurocode 3: design of steel structures – Part 1-1: general rules and rules for buildings [Authority: The European Union Per Regulation 305/2011, Directive 98/34/EC, Directive 2004/18/EC]. Brussels: European Comittee for Standardization; 2005. p. 93.
[16] Johnson GR, Cook WH. Fracture characteristics of three metals subjected to various strains, strain rates, temperatures and pressures. Eng Fract Mech 1985;21(1):31–48.
[17] Berriaud C, Dulac J, Sokolovsky A, Labrot R, Gueraud R, Avet-Flancard R. Local behaviour of reinforced concrete walls under missile impact. Nucl Eng Des 1978;45(2):457–69.
[18] Vu XV, Malecot Y, Daudeville L. Strain measurements on porous concrete samples for triaxial compression and extension test under very high confinement. J Strain Anal Eng Des 2009;44:633–57.
[19] Iqbal MA, Rai S, Sadique MR, Bhargava P. Numerical simulation of aircraft crash on nuclear containment structure. Nucl Eng Des 2012;44:321–35.
[20] Riech H, Rüdiger E. Versuchsergebnisse des Meppener Versuche II/11 bis II/2 (Results on MEPPEN tests II/11 to II/22), Technischer Bericht 1500 408 (RS 467). Brussels: European Comittee for Standardization; 1984. p. 93.
[21] NEA. In: IRSN, editor. Iris_2010, Improving robustness assessment methodologies for structures impacted by missiles, workshop proceedings. Brussels: European Comittee for Standardization; 2010. p. 93.